Progress In Electromagnetics Research, Vol. 134, 559–579, 2013

SPLIT-FIELD FINITE-DIFFERENCE TIME-DOMAIN SCHEME FOR KERR-TYPE NONLINEAR PERIODIC MEDIA

Jorge Francés[1, *], Jani Tervo[2], and Cristian Neipp[3]

[1]Department of Physics, Systems Engineering and Signal Theory, University of Alicante, San Vicente del Raspeig Drive, NW, Alicante, Ap. 99, E-3080, España

[2]Department of Physics and Mathematics, University of Eastern Finland, P. O. Box 111, FI-80101 Joensuu, Finland

[3]University Institute of Physics to Sciences and Technologies, University of Alicante, San Vicente del Raspeig Drive, NW, Alicante, Ap. 99, E-3080, España

Abstract—The Split-Field Finite-Difference Time-Domain (SF-FDTD) formulation is extended to periodic structures with Kerr-type nonlinearity. The optical Kerr effect is introduced by an iterative fixed-point procedure for solving the nonlinear system of equations. Using the method, formation of solitons inside homogenous nonlinear media is numerically observed. Furthermore, the performance of the approach with more complex photonic systems, such as high-reflectance coatings and binary phase gratings with high nonlinearity is investigated. The static and the dynamic behavior of the Kerr effect is studied and compared to previous works.

1. INTRODUCTION

The history of the nonlinear optics goes back as early as 1875 when Kerr [1] demonstrated the birefringence phenomenon in optically isotropic media under the effect of a DC biasing electric field. The same phenomenon takes place also due to the incoming field itself, in which case one speaks about the AC, or optical, Kerr effect [2, 3]. Mathematically, the Kerr effect can be described by the third-order nonlinear susceptibility $\chi_0^{(3)}$, which is non-negligible in a wide variety

Received 15 October 2012, Accepted 15 November 2012, Scheduled 7 December 2012
* Corresponding author: Jorge Francés Monllor (jfmonllor@ua.es).

of commonly used materials that can be integrated and used, e.g., in microelectronics, fiber optics, or optical waveguides in general. Even though the Kerr effect, being an intensity-dependent contribution to the electric permittivity, looks simple at first sight, its overall effect is actually quite complex. For example, different parts of an optical pulse are unequally affected by the Kerr-effect. One of the consequences of this is the optical soliton [2, 4–6], that arises from the balancing between the dispersion and the Kerr effect. Other implications of the effect include all-optical ultrafast applications, such as waveguides that combine linear media with nonlinear media [7] or all-optical switching devices utilizing nonlinear material [8]. In certain circumstances, periodic assemblies of nonlinear materials can exhibit a "latching" action, or bistability [9], rather like an electronic bistable logic circuit. The device operation is controlled by the light beam itself and it has been found to possess exotic properties such as the zero-n gap. This effect is achieved by means of alternating positive-index and negative-index materials. It was found that this zero-n gap is robust for scaling and omnidirectional for oblique incidence, which makes this type of structures very useful [10–14]. The properties of nonlinear materials and their effect in periodic structures have been also investigated for a wide range of applications [15].

Even though the third-order nonlinearity is relatively weak in most materials, especially if short propagation distances and relatively weak incident-light intensities are considered, confinement of the field in optical nanostructures may lead to enhancement of the effect [2, 16]. Hence optical devices based on the third-order nonlinearity may offer an attractive alternative solution for integrated optoelectronics [17–20]. Unfortunately, numerical modeling of such devices with non-negligible nonlinearity is very challenging, since techniques based on, e.g., the solution of the Nonlinear Schrödinger Equations (NLSE) [21] are not accurate enough, and rigorous methods like Finite Element Method (FEM) and the Finite-Difference Time-Domain (FDTD) must be used.

FDTD was introduced by Yee [22] in 1966, and it has been proven to be one of the most powerful numerical techniques in the modeling of micro and nanoscale optical devices [4, 23–27]. For example, the analysis of periodic structures can be easily performed by means of the Periodic Boundary Conditions (PBCs) if the input plane wave is incident to the structure normally. In the general case of oblique incidence, however, the phase shift between the periods must be considered. This can be done, e.g., by the multiple grid approach [28] or the Split-Field (SF) method [29]. These techniques are based on the field transformation to eliminate the phase shift (time delay) between adjacent periods [30], and recently they have been widely used in the

analysis of periodic structures [31–33].

Even though classical FDTD formulation has been extended to nonlinear media [4, 5, 23, 24, 34–36], the techniques to include nonlinearity in the algorithm are not directly applicable to the Split-Field formulation. In this paper, we present such an extension to the two-dimensional (2-D) SF-FDTD scheme, which admits efficient numerical modeling of one-dimensional (1-D) periodic structures with Kerr-type nonlinearity, even under oblique illumination. We first derive the theory for the split-field formulation with third-order nonlinearity, after which we present numerical examples for various types of structures.

2. THEORY

In this section, the basis for the SF-FDTD method and the implementation of the different add-ons are fully detailed. In the following discussion, we assume a structure that is periodic in the x direction, and that the input light field is a plane wave with wave vector $\mathbf{k}_{\text{inc}}$. We assume oblique incidence such that the wave vector forms an angle θ_0 with the positive z axis (see Fig. 1). In practice, the periodicity of the problem is introduced by applying periodic boundary conditions (PBC). Even though we restrict to one-dimensionally periodic structures for simplicity, extension to the general case is expected to be done straightforward (c.f. the split-field formulation for linear media in [32]). We also assume Uniaxial Perfectly Matched Layer [37, 38] (UPML) for the truncation in the z direction. The input plane wave source is excited in the structure following the schemes proposed in [23, 39] for both continuous and time-limited pulsed waves.

2.1. Basic Concepts of SF-FDTD

Let us next recall the derivation of SF-FDTD. We assume non-magnetic and non-conducting media, in which case Maxwell's curl equations take on the forms

$$\nabla \times \mathbf{E} = -\mu_0 \frac{\partial \mathbf{H}}{\partial t}, \tag{1}$$

$$\nabla \times \mathbf{H} = \frac{\partial \mathbf{D}}{\partial t}, \tag{2}$$

where μ_0 is the permeability of free space, and $\mathbf{D}$ and $\mathbf{H}$ are the time domain electric flux density and the magnetic field, respectively. It is convenient to split the electric flux density to the linear and nonlinear

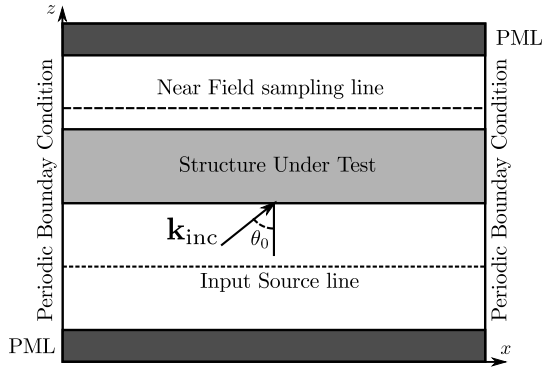

Figure 1. Scheme of a 2D computational space.

parts with

$$\mathbf{D} = \epsilon_0 \epsilon_r \mathbf{E} + \mathbf{F}^{\text{NL}}, \tag{3}$$

where ϵ_0 is the permittivity of free space, ϵ_r denotes the relative permittivity, and $\mathbf{F}^{\text{NL}}$ is the nonlinear polarization. Consequently, Eq. (2) can be rewritten as

$$\nabla \times \mathbf{H} = \epsilon_0 \epsilon_r \frac{\partial \mathbf{E}}{\partial t} + \mathbf{J}^{\text{NL}}, \tag{4}$$

where $\mathbf{J}^{\text{NL}}$ is the nonlinear polarization current density defined by $\partial \mathbf{F}^{\text{NL}} / \partial t$.

Since we have assumed a plane-wave illumination from oblique incidence, and the structure is periodic in the x direction, the field everywhere contains a linear x-dependent phase term $\exp(jk_x x)$, where $k_x = (\omega/c)\sin\theta_0$ is the x component of the wave vector in the phasor domain, ω is the angular frequency, and c is the speed of light in vacuum. In the SF formulation, we eliminate the effect of such a phase term using the transformation

$$\breve{\mathbf{P}} = \breve{\mathbf{E}} e^{jk_x x}, \tag{5}$$

$$\breve{\mathbf{Q}} = \mu_0 c \breve{\mathbf{H}} e^{jk_x x}, \tag{6}$$

where $\breve{\mathbf{P}}$ and $\breve{\mathbf{Q}}$ are the transformed vectors in the phasor domain. Analogous transformation can also be applied to $\breve{\mathbf{J}}^{\text{NL}}$ by introducing the new transformed vector variable $\breve{\mathbf{G}}^{\text{NL}}$:

$$\breve{\mathbf{G}}^{\text{NL}} = \mu_0 c \breve{\mathbf{J}}^{\text{NL}} e^{jk_x x} \tag{7}$$

Substituting Eqs. (5)–(7) into Maxwell's equations, the basis for the SF-FDTD can be expressed in its time-domain component-wise

form

$$\frac{1}{c}\frac{\partial P_x}{\partial t} = -\kappa\frac{\partial Q_y}{\partial z} - \kappa G_x^{\mathrm{NL}}, \tag{8}$$

$$\frac{1}{c}\frac{\partial P_y}{\partial t} = \kappa\left(\frac{\partial Q_x}{\partial z} - \frac{\partial Q_z}{\partial x}\right) + \sin\theta_0\frac{\kappa}{c}\frac{\partial Q_z}{\partial t} - \kappa G_y^{\mathrm{NL}}, \tag{9}$$

$$\frac{1}{c}\frac{\partial P_z}{\partial t} = \kappa\frac{\partial Q_y}{\partial x} - \sin\theta_0\frac{\kappa}{c}\frac{\partial Q_y}{\partial t} - \kappa G_z^{\mathrm{NL}}, \tag{10}$$

where $\mathbf{P}$ and $\mathbf{Q}$ are time-domain vectors, $\kappa = \epsilon_r^{-1}$, and

$$\frac{1}{c}\frac{\partial Q_x}{\partial t} = \frac{\partial P_y}{\partial z}, \tag{11}$$

$$\frac{1}{c}\frac{\partial Q_y}{\partial t} = \frac{\partial P_z}{\partial x} - \frac{\partial P_x}{\partial z} - \sin\theta_0\frac{1}{c}\frac{\partial P_z}{\partial t}, \tag{12}$$

$$\frac{1}{c}\frac{\partial Q_z}{\partial t} = -\frac{\partial P_y}{\partial x} + \sin\theta_0\frac{1}{c}\frac{\partial P_y}{\partial t}, \tag{13}$$

Following [29, 39], we next eliminate the time-derivative terms $\partial/\partial t \Leftrightarrow j\omega$ by splitting the field variables:

$$P_x = P_{xa} - c^2\mu_0\kappa F_x^{\mathrm{NL}} e^{jk_x x}, \tag{14}$$

$$P_y = P_{ya} + \sin\theta_0\kappa Q_z - c^2\mu_0\kappa F_y^{\mathrm{NL}} e^{jk_x x}, \tag{15}$$

$$P_z = P_{za} - \sin\theta_0\kappa Q_y - c^2\mu_0\kappa F_z^{\mathrm{NL}} e^{jk_x x}, \tag{16}$$

$$Q_x = Q_{xa}, \tag{17}$$

$$Q_y = Q_{ya} - \sin\theta_0 P_z, \tag{18}$$

$$Q_z = Q_{za} + \sin\theta_0 P_y, \tag{19}$$

Finally, substituting Eqs. (14)–(19) into the left-hand of Eqs. (8)–(13) results in equations for "a" fields:

$$\frac{1}{c}\frac{\partial P_{xa}}{\partial t} = -\kappa\frac{\partial Q_y}{\partial z}, \tag{20}$$

$$\frac{1}{c}\frac{\partial P_{ya}}{\partial t} = \kappa\left(\frac{\partial Q_x}{\partial z} - \frac{\partial Q_z}{\partial x}\right), \tag{21}$$

$$\frac{1}{c}\frac{\partial P_{za}}{\partial t} = \kappa\frac{\partial Q_y}{\partial x}, \tag{22}$$

and

$$\frac{1}{c}\frac{\partial Q_x}{\partial t} = \frac{\partial P_y}{\partial z}, \tag{23}$$

$$\frac{1}{c}\frac{\partial Q_{ya}}{\partial t} = \frac{\partial P_z}{\partial x} - \frac{\partial P_x}{\partial z}, \tag{24}$$

$$\frac{1}{c}\frac{\partial Q_{za}}{\partial t} = -\frac{\partial P_y}{\partial y}, \tag{25}$$

The periodic boundary conditions are now simply applied by forcing the field values at grid locations $\left(x = \Lambda + \frac{\Delta u}{2}\right)$ and $\left(x = \frac{\Delta u}{2}\right)$ to equal those at $\left(x = \frac{3\Delta u}{2}\right)$ and $\left(x = \Lambda - \frac{\Delta u}{2}\right)$. The constant Δu is defined in Subsection 2.2 and it is related with the spatial resolution of SF-FDTD. In the next subsection, we discuss the implementation of the Lorentz linear contribution in the permittivity and the polarization terms in Eqs. (14)–(16) for the specific case of third-order nonlinear media.

2.2. Kerr Model in SF-FDTD

In general, the third-order nonlinear polarization for the Kerr nonlinear effect is given either by

$$\mathbf{F}_{\text{Kerr}}(t) = \epsilon_0 \chi_0^{(3)} |\mathbf{E}|^2 \mathbf{E}, \tag{26}$$

where $\chi_0^{(3)}$ is the third-order dielectric susceptibility, or, equivalently, by

$$\mathbf{J}_{\text{Kerr}}(t) = \frac{\partial \mathbf{F}_{\text{Kerr}}}{\partial t} = \frac{\partial}{\partial t} \epsilon_0 \chi_0^{(3)} |\mathbf{E}|^2 \mathbf{E}. \tag{27}$$

Now, in SF-FDTD, we have [32]

$$\mathbf{P}\mathbf{P}^* = \mathbf{E}\mathbf{E}^* = |\mathbf{E}|^2. \tag{28}$$

Further, due to the linear relation between $\mathbf{J}_{\text{Kerr}}$ and $\mathbf{E}$, the transformation into the split-field domain is straightforward:

$$\breve{\mathbf{G}}_K = \mu_0 c \breve{\mathbf{J}}_{\text{K}} e^{jk_x x} = \frac{j\omega}{c} \chi_0^{(3)} |\breve{\mathbf{E}}|^2 \breve{\mathbf{P}}, \tag{29}$$

If we denote the transformed linear polarization current in the Lorentz model [33] by $\breve{\mathbf{G}}_L$, we may now reformulate Eqs. (8)–(10) in Lorentz media and with the new contribution from the Kerr-type nonlinearity discussed above:

$$\frac{1}{c}\frac{\partial P_x}{\partial t} = -\kappa \left[\frac{\partial Q_y}{\partial z} + G_{Lx} + \frac{1}{c}\chi_0^{(3)} \frac{\partial |E_x|^2 P_x}{\partial t} \right], \tag{30}$$

$$\frac{1}{c}\frac{\partial P_y}{\partial t} = \kappa \left[\left(\frac{\partial Q_x}{\partial z} - \frac{\partial Q_z}{\partial x} \right) + \frac{1}{c} \sin\theta_0 \frac{\partial Q_z}{\partial t} - G_{Ly} - \frac{1}{c}\chi_0^{(3)} \frac{\partial |E_y|^2 P_y}{\partial t} \right], \tag{31}$$

$$\frac{1}{c}\frac{\partial P_z}{\partial t} = \kappa \left[\frac{\partial Q_y}{\partial x} - \frac{1}{c} \sin\theta_0 \frac{\partial Q_y}{\partial t} - G_{Lz} - \frac{1}{c}\chi_0^{(3)} \frac{\partial |E_z|^2 P_z}{\partial t} \right], \tag{32}$$

For updating the equations, the Kerr terms must be considered after updating the "a" fields, since Kerr effect requires solving a nonlinear

system of coupled equations that depends on **P**. Hence, Eqs. (14)–(16) should be reformulated as follows:

$$P_x = P_{xa} - \chi_0^{(3)}\kappa|E_x|^2 P_x, \tag{33}$$

$$P_y = P_{ya} + \sin\theta_0\kappa Q_z - \chi_0^{(3)}\kappa|E_y|^2 P_y, \tag{34}$$

$$P_z = P_{za} - \sin\theta_0\kappa Q_y - \chi_0^{(3)}\kappa|E_z|^2 P_z, \tag{35}$$

where P_{ma}, with $m = x, y$ or z are given by Eqs. (20)–(22) in nondispersive media and by the following update equations

$$P_{xa}|_{i+\frac{1}{2},k}^{e+1} = P_{xa}|_{i+\frac{1}{2},k}^{e} - \kappa\left[S\left(Q_y|_{i+\frac{1}{2},k+\frac{1}{2}}^{e+\frac{1}{2}} - Q_y|_{i+\frac{1}{2},k-\frac{1}{2}}^{e+\frac{1}{2}}\right) + c\Delta t G_{Lx}|_{i+\frac{1}{2},k}^{e+\frac{1}{2}}\right] \tag{36}$$

$$P_{ya}|_{i,k}^{e+1} = P_{ya}|_{i,k}^{e} + \kappa\left[S\left(Q_x|_{i,k+\frac{1}{2}}^{e+\frac{1}{2}} - Q_x|_{i,k-\frac{1}{2}}^{e+\frac{1}{2}} - Q_z|_{i+\frac{1}{2},k}^{e+1/2} + Q_z|_{i-\frac{1}{2},k}^{e+1/2}\right) - c\Delta t G_{Ly}|_{i,k}^{e+\frac{1}{2}}\right], \tag{37}$$

$$P_{za}|_{i,k+\frac{1}{2}}^{e+1} = P_{za}|_{i,k+\frac{1}{2}}^{e} + \kappa\left[S\left(Q_y|_{i+\frac{1}{2},k+\frac{1}{2}}^{e+\frac{1}{2}} - Q_y|_{i-\frac{1}{2},k+\frac{1}{2}}^{e+\frac{1}{2}}\right) + c\Delta t G_{Lz}|_{i,k+\frac{1}{2}}^{e+\frac{1}{2}}\right]. \tag{38}$$

in Lorentz media, respectively. In these equations, $S = c\Delta t/\Delta u$, being Δu and Δt the spatial and time resolutions respectively. The integers i, k denote the position of sample points in x and z axis whereas the integeer e localizes a determined time step. The update formula for $\mathbf{G}_L$ is fully detailed in [33].

The update step of the total fields given in Eqs. (14)–(19) can be reformulated removing the temporal dependencies properly and using only the "a" fields:

$$P_z = \frac{P_{za} - \kappa\sin\theta_0 Q_{ya}}{1 + \kappa\left(\chi_0^{(3)}|E_z|^2 - \sin^2\theta_0\right)} = C_z\hat{P}_{za}, \tag{39}$$

$$Q_y = Q_{ya} - \sin\theta_0 P_z, \tag{40}$$

$$P_x = \frac{P_{xa}}{1 + \kappa\chi_0^{(3)}|E_x|^2} = C_x P_{xa}, \tag{41}$$

$$P_y = \frac{P_{ya} + \kappa\sin\theta_0 Q_{za}}{1 + \kappa\left(\chi_0^{(3)}|E_y|^2 - \sin^2\theta_0\right)} = C_y\hat{P}_{ya}, \tag{42}$$

$$Q_z = Q_{za} + \sin\theta_0 P_y, \tag{43}$$

where C_m are the update coefficients defined in

$$C_x = \frac{1}{1+\kappa\chi_0^{(3)} I_x}, \tag{44}$$

$$C_y = \frac{1}{1+\kappa\left(\chi_0^{(3)} I_y - \sin^2\theta_0\right)}, \tag{45}$$

$$C_z = \frac{1}{1+\kappa\left(\chi_0^{(3)} I_z - \sin^2\theta_0\right)}, \tag{46}$$

and

$$\mathbf{I} = |\mathbf{E}|^2. \tag{47}$$

To update $\mathbf{I}$ in each time step, a fixed point iteration has to be performed. The general equation for such a fixed point iteration is $\mathbf{I}|_{p+1} = \mathbf{P}|_p \left(\mathbf{P}|_p\right)^*$ that can be extended for each space coordinate

$$I_x|_{p+1} = C_x|_p \left(C_x|_p\right)^* |P_{xa}|^2, \tag{48}$$

$$I_y|_{p+1} = C_y|_p \left(C_y|_p\right)^* |\hat{P}_{ya}|^2, \tag{49}$$

$$I_z|_{p+1} = C_z|_p \left(C_z|_p\right)^* |\hat{P}_{za}|^2, \tag{50}$$

where

$$C_x|_p = \frac{1}{1+\kappa\chi_0^{(3)} I_x|_p}, \tag{51}$$

$$C_y|_p = \frac{1}{1+\kappa\left(\chi_0^{(3)} I_y|_p - \sin^2\theta_0\right)}, \tag{52}$$

$$C_z|_p = \frac{1}{1+\kappa\left(\chi_0^{(3)} I_z|_p - \sin^2\theta_0\right)}, \tag{53}$$

are updated in each iteration. Note that in this case, the subindex p is an integer related with the iteration step for the fixed point iteration process, not for the spatial dimension. The fixed point iteration, which requires the most computational time of the updating process, can be skipped when the Kerr effect is negligible. The convergence of the fixed point iteration is proven using Banach's fixed point theorem [40] that, in the case of normal incidence, takes on the form

$$\left[\left(\epsilon_r + \chi_0^{(3)} I\right) E\right]^2 \chi_0^{(3)} \leq \frac{\epsilon_r^3}{2}. \tag{54}$$

The amplitude of the electric field E has to be limited to an upper value that is related with the amplitude of the third-order susceptibility

$\chi_0^{(3)}$ to assure convergence of the fixed point iteration. Regarding the iterative process, an experimental procedure was done in order to establish an upper limit in the number of iteration. Here, the maximum number of iteration has been fixed to 30 steps achieving good results near the upper limit of convergence of the method [40].

3. RESULTS

In this section, we discuss the results derived from the analysis of nonlinear media. Firstly, we show simulations of temporal solitons, and compare them with results presented in the literature [4–6, 23]. Secondly, we analyze both DC and AC Kerr effects by means of the reflectance analysis of different stack of layers with nonlinear characteristics. Finally, we illustrate the full potential of the SF-FDTD scheme with the analysis of binary phase gratings made of nonlinear strips, employing both the normal and oblique incidences.

3.1. Simulation of Temporal Solitons

To validate the results given by the method introduced in the preceding section, we study the interaction of a pulsed optical-signal source switched on at $t = 0$ at the surface $z = 0$ of a material having linear dispersive properties. The source is defined as a bandpass Gaussian pulse with zero DC component and a planar wavefront perpendicular to the direction of propagation is considered. The pulse has a maximum absolute amplitude of 1.1 V/m with a carrier frequency $f_c = 1.37 \cdot 10^{14}$ Hz ($\lambda_0 = 2.19\,\mu$m). Approximately three cycles of the optical carrier were contained within the pulse envelope. To demonstrate soliton formation over short propagations spans of less than 150 µm, we chose the parameters following the work of Joseph et al. [4]:

- Linear dispersion: $\epsilon_s = 5.25$, $\epsilon_\infty = 2.25$, $\omega_L = 4 \cdot 10^{14}\,\mathrm{s}^{-1}$, $\gamma_L = 2 \cdot 10^9\,\mathrm{s}^{-1}$.
- Nonlinear material: $\chi_0^{(3)} = 7 \cdot 10^{-2}\,(\mathrm{V/m})^{-2}$.

We chose the spatial resolution to be 52.5 nm ($\approx \lambda_0/40$), whereas the time resolution Δt was obtained by employing the so called "Courant condition", which gives $\Delta t = \Delta u/(\sqrt{2}c_0) = 129.64 \cdot 10^{-9}$ ns.

Figure 2 depicts the results of the dispersive and nonlinear SF-FDTD computations. In Fig. 2(a) the computed pulse for the linear Lorentz dispersive is graphed at $t = 2000\Delta t$ and $4000\Delta t$. It is clear that the assumed linear dispersion caused substantial broadening of the computed pulse along with diminishing amplitude

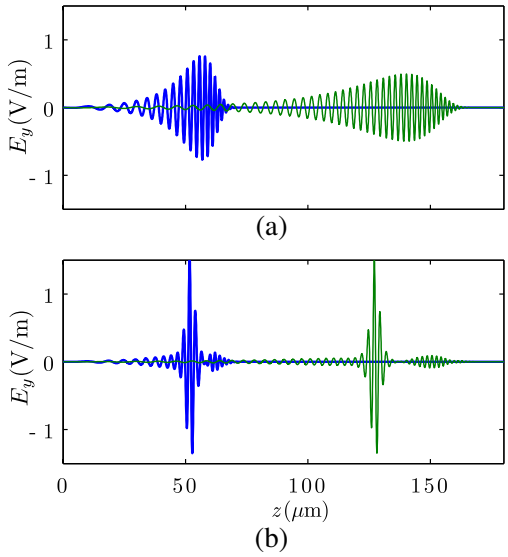

Figure 2. Snapshots of the electric field $\Re\{E_y\}$ in different kind of mediums detected from left to right at times $t = 2000\Delta t$ (thick line) and $t = 4000\Delta t$ (thin line) respectively. (a) Linear dispersive Lorentz media. (b) Nonlinear Lorentz and Kerr media.

and carrier frequency modulation, being greater on the leading side of the pulse, and minor on the trailing side of the pulse. Fig. 2(b) shows the pulse propagation when the Kerr effect is included in the simulations. As can seen from the figure, a temporal soliton and also a smaller-magnitude precursor-pulse, that is identified as transient third-harmonic energy, are formed. These results reproduce those presented in the literature [4–6].

3.2. Electro-Optic Kerr Effect

Consider next a superposition of a DC electric field E_{ext} and linearly polarized optical field, with its plane of vibration in the y direction, propagating in Kerr-type medium. Solving the nonlinear wave equation for this case, it is possible to describe accurately the behavior of the electric field using the concept of the effective nonlinear refractive index of the form

$$n_{\text{eff}} = n_0 + 3\chi_0^{(3)} E_{\text{ext}}^2 + \frac{3\chi_0^{(3)} E_y^2}{4}, \tag{55}$$

where n_0 is a linear refractive index of the medium. The mathematical process in order to obtain (55) is fully detailed in [16]. In Eq. (55), the first two terms describe the linear response and the DC Kerr effect, respectively, whereas the last term gives us the familiar all-optical AC Kerr nonlinear response. In the following, we analyze the static effect with low optical-field intensity.

We first apply the SF-FDTD to a short thin-film Bragg-type reflector, i.e., a stack of layers with $\lambda/4$ optical thickness, and with alternating high and low refractive indices (see Fig. 3). The nonlinear material is located in the high refractive index material and its value has been chosen in order to trigger the nonlinearity following the scheme detailed in the work of Pinto et al. [41]. In FDTD computations and nonlinear media is very common to scale the susceptibility terms in order to trigger the nonlinearity with lower intensities reducing

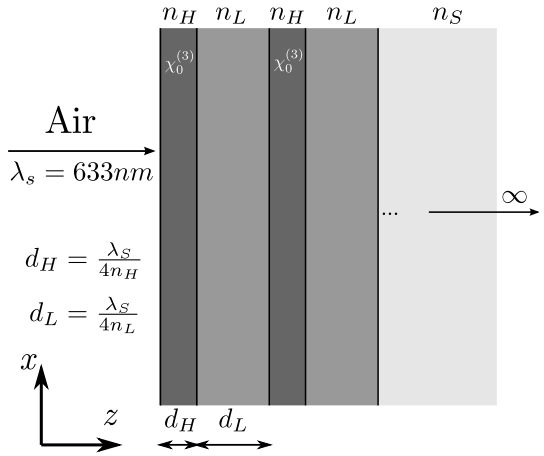

Figure 3. Scheme of a high-reflection coating.

Table 1. Setup parameters of SF-FDTD for results in Fig. 4.

λ_0 (nm)	Δu (m)	Δt (s)	r_x (cells)	r_z (cells)	r_{PML} (cells)	e_{steps}
500	$\lambda_0/80$	$\Delta u/(\sqrt{2}c_0)$	20	500	40	1000

Table 2. Parameters of the Bragg reflector with nonlinear materials (static analysis).

n_H	n_L	n_{Glass}	$\chi_0^{(3)}$ (m/V)^2	λ_S (nm)
2.3	1.38	1.52	500	633

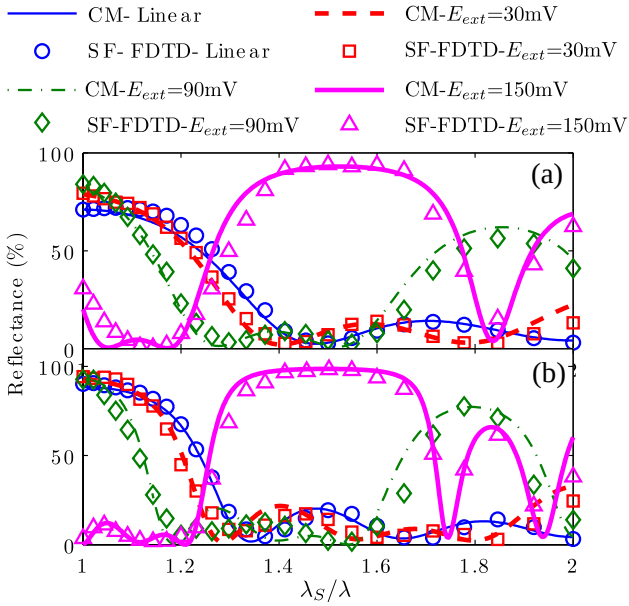

Figure 4. Reflectance for two high reflection coatings. (a) Air $|HL|^2G$. (b) Air$|HL|^3G$.

roundoff errors [4, 23, 34, 35]. The SF-FDTD setup for this experiment is summarized in Table 1, whereas the physical values of the parameters are listed Table 2.

Figure 4 shows the reflectance of the structure. The number of periods are two for Fig. 4(a) and three for Fig. 4(b). In both cases the numerical samples obtained by SF-FDTD are compared with the theoretical curves obtained by the Characteristic Matrix (CM) method detailed in [42]. One can see from the figure that the external DC electric field controls the amplitude-reflectance, as well as the lower and upper cut-offs of the band edges. When the amplitude of the DC field becomes considerably greater, the number of secondary lobes and their amplitude become also relevant. In both cases the numerical and theoretical values are close.

3.3. Dynamic Kerr Effect

Let us next repeat the analysis of the Bragg-type reflector discussed in the preceding subsection, but now with no external DC field and with considerable intensity of the optical field. To work with realistic intensities, the physical parameters have been modified. The new

parameters regarding SF-FDTD setup and physical values are listed in Table 3 and Table 4 respectively. Here the third-order susceptibility of both materials is non-zero.

Figures 5(a)–(f) show the reflectance as a function of the parameter λ_S/λ for the two-period case, whereas Figs. 5(g)–(l) represent the results with three periods. In both cases, as the input source intensity becomes greater the differences between SF-FDTD (circles) results and those obtained by means of the CM method (solid

Table 3. Setup parameters of SF-FDTD for results in Fig. 5.

λ_0 (nm)	Δu (m)	Δt (s)	r_x (cells)	r_z (cells)	r_{PML} (cells)	e_{steps}
316.5	$\lambda_0/200$	$\Delta u/(\sqrt{2}c_0)$	6	750	100	1600

Table 4. Parameters of the Bragg-reflector with nonlinear materials (dynamic analysis) [2].

Polymer		Fused Silica		Glass
n_H	$\chi_H^{(3)}$ (m/V)^2	n_L	$\chi_L^{(3)}$ (m/V)^2	n_G
2.81	$5.6{\cdot}10^{-16}$	1.47	$2.5{\cdot}10^{-22}$	1.52

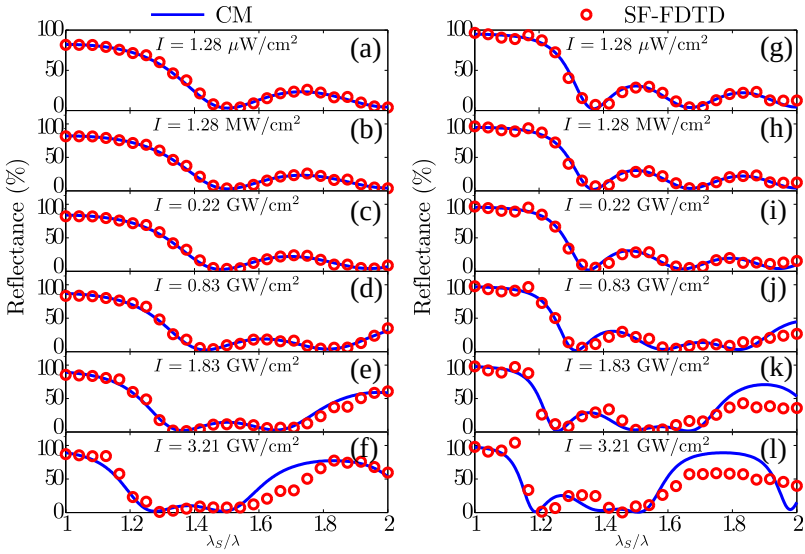

Figure 5. Reflectance for two high reflection coatings with different input source intensities. (a)–(h) Air|HL|^{2}G. (g)–(l) Air|HL|^{3}G.

line) also tend to be relevant. The solid curves are obtained considering an effective refractive index in the third term of Eq. (55) and neglecting the second term. This refractive index is the input parameter in CM. As the input source intensity increases the dynamic behaviour related with the nonlinear materials also grows and thus the differences between the dynamic analysis performed by SF-FDTD and the static performed by CM.

3.4. Binary Phase Gratings

Finally, we turn to investigate structures that are periodic in lateral direction, namely binary phase gratings, illustrated in Fig. 6. Throughout the analysis, we assume 50% fill factor, and the nonlinear material is assumed to be in the pillars only. As is logical in SF-FDTD, only one period is needed in the simulations. The grating parameters are given in Table 5.

Figure 7 shows the zeroth-order (η_0) and the first-orders ($\eta_{\pm 1}$) efficiencies with different input intensities. The efficiency curves are slightly modified as the input source intensity is increased. Of course, even higher intensities would lead to more radical effects but, in this particular example, we kept the intensities in realistic values for assumed polymer material to show what kind of effect can be expected to be observed in the practice.

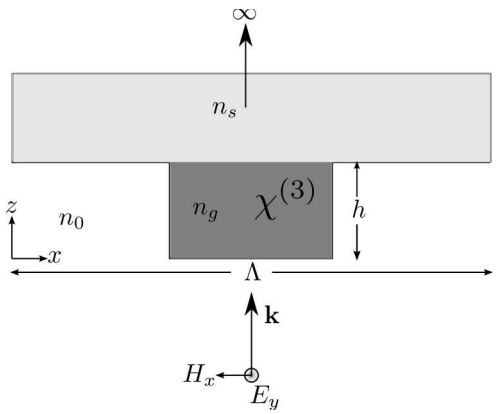

Figure 6. Binary grating scheme.

Table 5. Setup parameters of SF-FDTD for results in Fig. 7.

λ_0 (nm)	Δu (m)	Δt (s)	r_x (cells)	r_z (cells)	r_{PML} (cells)	e_{steps}
633	$\lambda_0/60$	$\Delta u/(\sqrt{2}c_0)$	150	400	30	1000

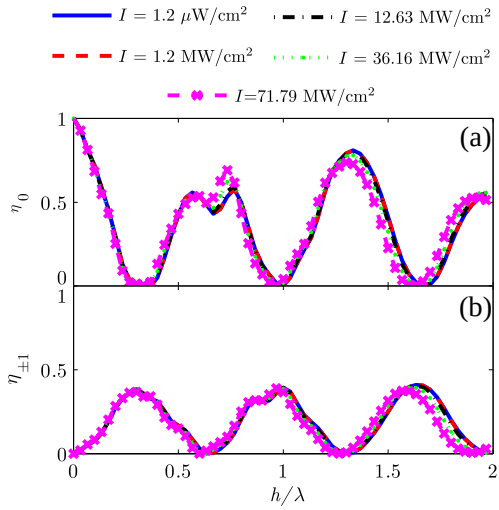

Figure 7. Diffraction efficiencies with different input source intensities. (a) Zero order. (b) First order. Parameters: $\Delta/\lambda_0 = 2.5$, $n_g = 2.48$, $n_s = 1.47$, $\chi_0^{(3)} = 5.6 \cdot 10^{-16}$ (m/V)^2.

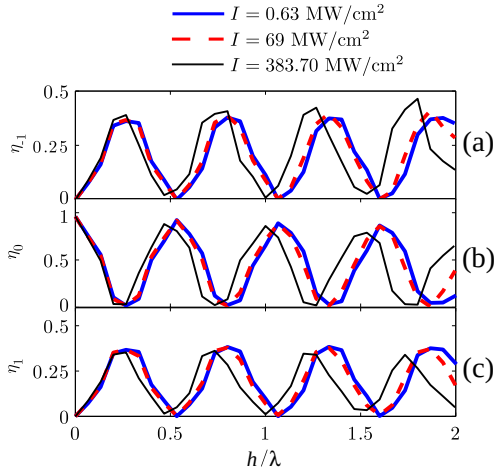

Figure 8. Diffraction efficiencies with different input source intensities. (a) Minus first-order. (b) Zero-order. (c) First-order. Parameters: $\Lambda/\lambda_0 = 20$, $n_g = 2.81$, $n_s = 1.47$, $\chi_0^{(3)} = 5.6 \cdot 10^{-16}$ (m/V)^2.

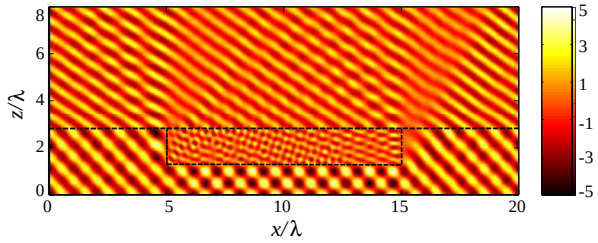

Figure 9. Electric Field distribution (E_y) in MV/m as a function of the space for a binary phase grating. Parameters: $\Lambda/\lambda_0 = 20$, $h/\lambda_0 = 1.8$, $n_g = 2.81$, $n_s = 1.47$, $\chi_0^{(3)} = 5.6 \cdot 10^{-16}\,(\mathrm{m/V})^2$.

Table 6. Setup parameters of SF-FDTD for results in Figs. 8–9.

λ_0 (nm)	Δu (m)	Δt (s)	r_x (cells)	r_z (cells)	r_{PML} (cells)	e_{steps}
633	$\lambda_0/30$	$0.567\Delta u/(c_0)$	600	400	15	1200

We also performed the analysis with oblique angle of incidence for a binary grating with period $\Lambda = 20\lambda$ at 30°. The diffraction efficiencies are shown in Fig. 8. As with the normal incidence, the influence of the nonlinear material is relatively small with the assumed combination of the input-field intensity and the third-order susceptibility.

To further illustrate the potential of the SF-FDTD approach, a distribution of the electric field is also shown in Fig. 9. As can be seen from the figure, the SF-FDTD can easily perform simulations with large periods without excess computational burden, which is not the case with the standard Yee FDTD scheme that requires inclusion of several periods in the computation. Namely, as is well known, the simulation time and required memory grows extremely rapidly as a function of the dimensions of the computation grid, and hence the use of SF-FDTD approach in the analysis of laterally periodic structures is strongly preferred over the classical FDTD.

4. CONCLUSIONS AND OUTLOOK

In this paper, we extended the Split-Field Finite-Difference Time-Domain to periodic optical media with third-order nonlinearity. This enables accurate modeling of the AC Kerr effect, which is particularly important in numerous areas of nonlinear optics. In this method, the third-order susceptibility is included using the concept of the

polarization current that requires solving of a nonlinear system of equations. Hence a fixed-point iterative procedure is needed to compute the components of the transformed split-field variables related with the electric field.

We validated the method numerically by comparisons to already-known structures and phenomena, including temporal solitons in homogeneous medium and the DC Kerr effect in short Bragg-type reflector. We then showed the efficiency of the method by analyzing the Bragg-reflector with AC Kerr effect and, finally, by simulations of binary phase gratings with nonlinearity, in both normal and oblique incidence.

The authors are currently working on extending the approach to anisotropic materials. The computational resources required by the SF-FDTD in anisotropic media must be considered. Therefore authors are also working on acceleration strategies based on multi-core CPUs and GPU computing.

ACKNOWLEDGMENT

The work is partially supported by the Academy of Finland (project 118951), the Strategic Funding of the University of Eastern Finland, by the "Ministerio de Economía y Competitividad" of Spain under project FIS2011-29803-C02-01 and by the "Generalitat Valenciana" of Spain under projects PROMETEO/2011/021 and ISIC/2012/013.

REFERENCES

1. Kerr, J., "A new relation between electricity and light: Dielectrified media birefringent," *Phil. Mag. J. Sci.*, Vol. 50, No. 3, 337–393, 1875.
2. Boyd, R. W., *Nonlinear Optics*, 2nd Edition, Academic Press, 2003.
3. Aberg, I., "High-frequency switching and Kerr effect — Nonlinear problems solved with nonstationary time domain techniques — Summary," *Journal of Electromagnetic Waves and Applications*, Vol. 12, No. 1, 85–90, 1998.
4. Joseph, R. M. and A. Taflove, "FDTD Maxwell's equations models for nonlinear electrodynamics and optics," *IEEE Trans. Antennas Propag.*, Vol. 45, No. 3, 364–374, 1997.
5. Kosmidou, E. P. and T. D. Tsiboukis, "An unconditionally stable ADI-FDTD algorithm for nonlinear materials," *Proc. ISTET*, 2003.

6. Fujii, M., M. Tahara, I. Sakagami, W. Freude, and P. Russer, "High-order FDTD and auxiliary differential equation formulation of optical pulse propagation," *IEEE J. Quantum Electron.*, Vol. 40, No. 2, 175–182, 2004.
7. Balourdos, P. S., D. J. Frantzeskakis, M. C. Tsilis, and I. G. Tigelis, "Reflectivity of a nonlinear discontinuity in optical waveguides," *Journal of Optics A: Pure and Applied Optics*, Vol. 7, No. 1, 1–11, 1998.
8. Deering, W. D. and G. M. Molina, "Power switching in hybrid coherent couplers," *IEEE J. Quantum Electron.*, Vol. 33, No. 3, 336–340, 1998.
9. Zhou, F., Y. Liu, Z.-Y. Li, and Y. Xia, "Analytical model for optical bistability in nonlinear metal nano-antennae involving Kerr materials," *Opt. Express*, Vol. 18, No. 15, 13337–13344, 2010.
10. Wang, S. M. and L. Gao, "Nonlinear responses of the periodic structure composed of single negative materials," *Opt. Commun.*, Vol. 267, No. 1, 197–204, 2006.
11. Wang, S. M., C. G. Tang, T. Pan, and L. Gao, "Bistability and gap soliton in one-dimensional photonic crystal containing single-negative materials," *Phys. Lett. A*, Vol. 348, Nos. 3–6, 424–431, 2006.
12. Hedge, R. S. and H. G. Winful, "Optical bistability in periodic nonlinear structures containing left handled materials," *Microw. Opt. Technol. Lett.*, Vol. 46, No. 36, 528–530, 2005.
13. Gao, D. and L. Gao, "Goos-Hänchen shift of the reflection from nonlinear nanocomposites with electric field tunability," *Appl. Phys. Lett.*, Vol. 97, 041903, 2010.
14. Dong, W., L. Gao, and C.-W. Qiu, "Goos-Hänchen shift at the surface of chiral negative refractive media," *Progress In Electromagnetic Research*, Vol. 90, 255–268, 2009.
15. Brzozowski, L. and E. H. Sargent, "Optical signal processing using nonlinear distributed feedback structures," *IEEE J. Quantum Electron.*, Vol. 36, No. 5, 550–555, 2000.
16. Qasymeh, M., M. Cada, and S. A. Ponomarenko, "Quadratic electro-optic Kerr effect: Applications to photonic devices," *IEEE J. Quantum Electron.*, Vol. 44, No. 8, 740–746, 2008.
17. Wu, J.-W. and H.-B. Bao, "Simultaneous generation of ultrafast bright and dark pulse employing nonlinear processes based on the silicon waveguides," *Journal of Electromagnetic Waves and Applications*, Vol. 23, Nos. 8–9, 1143–1154, 2009.
18. Li, Y. E. and X. P. Zhang, "Nonlinear optical switch utilizing long-

range surface plasmon polaritons," *Journal of Electromagnetic Waves and Applications*, Vol. 23, Nos. 17–18, 2363–2371, 2009.

19. Crutcher, S., A. Biswas, M. D. Aggarwal, and M. E. Edwards, "Oscillatory behavior of spatial solitons in two-dimensional waveguides and stationary temporal power law solitons in optical fibers," *Journal of Electromagnetic Waves and Applications*, Vol. 20, No. 6, 761–772, 2006.
20. Ghafoori-Fard, H., M. J. Moghimi, and A. Rostami, "Linear and nonlinear superimposed Bragg grating: A novel proposal for all-optical multi-wavelength filtering and switching," *Progress In Electromagnetic Research*, Vol. 77, 243–266, 2007.
21. Morgan, S. A., R. J. Ballagh, and K. Burnett, "Solitary-wave solutions to nonlinear Schrödinger equations," *Phys. Rev. A*, Vol. 55, No. 6, 4338–4345, 1997.
22. Yee, K. S., "Numerical solution of initial boundary value problems involving Maxwell's equations in isotropic media," *IEEE Trans. Antennas Propag.*, Vol. 14, No. 3, 302–307, 1966.
23. Taflove, A. and S. C. Hagness, *Computational Electrodynamics: The Finite-Difference Time-Domain Method*, Artech House, Norwood, MA, 2004.
24. Lee, K. H., I. Ahmed, R. S. M. Goh, E. H. Khoo, E. P. Li, and T. G. G. Hung, "Implementation of the FDTD method based on Lorentz-Drude dispersive model on GPU for plasmonics applications," *Progress In Electromagnetic Research*, Vol. 116, 441–456, 2011.
25. Francés, J., C. Neipp, M. Pérez-Molina, and A. Beléndez, "Rigorous interference and diffraction analysis of diffractive optic elements using the finite-difference time-domain method," *Comput. Phys. Commun.*, Vol. 181, No. 12, 1963–1973, 2010.
26. Francés, J., C. Neipp, A. Márquez, A. Beléndez, and I. Pascual, "Analysis of reflection gratings by means of a matrix approach," *Progress In Electromagnetic Research*, Vol. 118, 167–183, 2011.
27. Kalaee, P. and J. Rashed-Mohassel, "Investigation of dipole radiation pattern above a chiral media using 3D BI-FDTD approach," *Journal of Electromagnetic Waves and Applications*, Vol. 23, No. 1, 75–86, 2009.
28. Kao, Y. C. and R. G. Atkins, "A finite-difference time-domain approach for frequency selective surfaces at oblique incidence," *Proceedings of Antennas and Propagation Society International Symposium*, 1432–1435, 1996.
29. Roden, J. A., S. D. Gedney, M. P. Kesler, J. G. Maloney,

and P. H. Harms, "Time-domain analysis of periodic structures at oblique incidence: Orthogonal and nonorthogonal FDTD implementation," *IEEE Trans. Microw. Theory Tech.*, Vol. 46, No. 4, 420–427, 1998.

30. Veysoglu, M. E., R. T. Shin, and J. A. Kong, "A finite-difference time-domain analysis of wave scattering from periodic surfaces: Oblique incidence case," *Journal of Electromagnetic Waves and Applications*, Vol. 7, No. 12, 1595–1607, 1993.
31. Mao, Y., B. Chen, H.-Q. Liu, J.-L. Xia, and J.-Z. Tang, "A hybrid implicit-explicit spectral FDTD scheme for oblique incidence problems on periodic structures," *Progress In Electromagnetic Research*, Vol. 128, 153–170, 2012.
32. Shahmansouri, A. and B. Rashidian, "Comprehensive three-dimensional split-field finite-difference time-domain method for analysis of periodic plasmonic nanostructures: Near- and far-field formulation," *J. Opt. Soc. Am. B.*, Vol. 28, No. 11, 2690–2700, 2011.
33. Shahmansouri, A. and B. Rashidian, "GPU implementation of split-field finite-difference time-domain method for Drude-Lorentz dispersive media," *Progress In Electromagnetic Research*, Vol. 125, 55–77, 2012.
34. Goorjian, P. M., A. Taflove, R. M. Joseph, and S. C. Hagness, "Computational modeling of femtosecond optical solitons from Maxwell's equations," *IEEE J. Quantum Electron.*, Vol. 28, No. 10, 2416–2422, 1992.
35. Goorjian, P. M. and A. Taflove, "Direct time integration of Maxwell's equations in nonlinear dispersive media for propagation and scattering of femtosecond electromagnetic solitons," *Opt. Lett.*, Vol. 17, No. 3, 180–182, 1992.
36. Zhang, Y.-Q. and D.-B. Ge, "A unified FDTD approach for electromagnetic analysis of dispersive objects," *Progress In Electromagnetic Research*, Vol. 96, 155–172, 2009.
37. Gedney, S. D., "An anisotropic perfectly matched layer-absorbing medium for the truncation of FDTD lattices," *IEEE Trans. Antennas Propag.*, Vol. 44, No. 12, 1630–1639, 1996.
38. Zheng, G., A. A. Kishk, A. W. Glisson, A. B. Yakovlev, "Implementation of Mur's absorbing boundaries with periodic structures to speed up the design process using finite-difference time-domain method," *Progress In Electromagnetic Research*, Vol. 58, 101–114, 2006.
39. Oh, C. and M. Escuti, "Time-domain analysis of periodic anisotropic media at oblique incidence: An efficient FDTD

implementation," *Opt. Express*, Vol. 14. No. 24, 11870–11884, 2006.

40. Ammann, M., "Non-trivial materials in EM-FDTD," Master's Thesis, Department of Physics, Swiss Federal Institute of Technology, 2007.
41. Pinto, D., S. S. A. Obayya, B. M. A. Rahman, and K. T. V. Grattan, "FDTD analysis of nonlinear Bragg grating based optical devices," *Opt. Quant. Electron.*, Vol. 38, No. 15, 1217–1238, 2006.
42. Macleod, H. A., *Thin-Film Optical Filters*, 2nd Edition, Taylor & Francis, 2001.